INTERNATIONAL JOURNAL OF CHEMICAL REACTOR ENGINEERING

Volume 1 2003 *Article* A54

Modelling of a Reverse Flow Catalytic Membrane Reactor for the Partial Oxidation of Methane

J. Smit* M. van Sint Annaland†

J.A.M. Kuipers‡

*University of Twente, J.Smit@ct.utwente.nl

†University of Twente, M.vansintannaland@ct.utwente.nl

‡University of Twente, J.A.M.Kuipers@ct.utwente.nl

ISSN 1542-6580

Modelling of a Reverse Flow Catalytic Membrane Reactor for the Partial Oxidation of Methane

J. Smit, M. van Sint Annaland, and J.A.M. Kuipers

Abstract

Gas-To-Liquid (GTL) processes have great potential as alternative to conventional oil and coal processing for the production of liquid fuels. In GTL-processes the partial oxidation of methane (POM) is combined with the Fischer-Tropsch reaction. An important part of the investment costs of a conventional GTL-plant is related to cryogenic air separation. These costs could be substantially reduced by separating air with recently developed oxygen perm-selective perovskite membranes, which operate at similar temperatures as a POM reactor. Integration of these membranes in the POM reactor seems very attractive because oxygen reacts at the membrane surface resulting in a high driving force over the membrane increasing the oxygen permeation.

Because the POM-reaction is only slightly exothermic, the natural gas and air feed have to be preheated to high operating temperatures to obtain high syngas yields and because the Fischer-Tropsch reactor operates at much lower temperatures, recuperative heat exchange is essential for an air-based POM process. External heat transfer at elevated temperatures is expensive and therefore recuperative heat exchange is preferably carried out inside the reactor, which can be achieved with the reverse flow concept. To combine the POM reaction, air separation and recuperative heat exchange in a single apparatus a novel, multi-functional reactor is proposed, called the Reverse Flow Catalytic Membrane Reactor (RFCMR). In this reactor a relatively uniform temperature profile should be established at the membrane section and the temperature fronts should be located in the inert in- and outlet sections.

To study the RFCMR concept, reactor models have been developed assuming a shell-and-tube geometry, based on models that are commonly used to describe conventional reverse flow reactors. Simulations of the novel reactor concept revealed that a small amount of methane has to combusted on the air side to create

the reverse flow behaviour. Also a small amount of steam has to be injected distributively along the perovskite membrane section to maintain the centre of the reactor at nearly isothermal conditions. With these modifications it was found that the desired temperature profile could indeed be created in the RFCMR and that high overall syngas yields can be achieved.

KEYWORDS: reverse flow, catalytic membrane reactor, partial oxidation, syngas, reactor modelling

1 INTRODUCTION

Natural gas has a great potential as feedstock for liquid fuels as alternative to conventional oil and coal processing. A promising process to convert natural gas to liquid fuels is the so-called Gas-To-Liquid (GTL) process, in which the partial oxidation of methane (POM) to syngas (1) is followed by the Fischer-Tropsch reaction (2):

$$CH_4 + \tfrac{1}{2}O_2 \rightarrow CO + 2H_2 \quad (1)$$

$$nCO + 2nH_2 \rightarrow (CH_2)_n + nH_2O \quad (2)$$

POM-processes have been subject of research for over half a century (Prettre et al., 1946), but have not found widespread application yet in GTL-processes. An important part of the investment costs of a POM-process is related to cryogenic air separation (e.g. Rostrup-Nielsen, 2002). An alternative air separation could therefore substantially reduce these costs.

Air separation has recently also become possible with O_2 perm-selective perovskite membranes (e.g. Bouwmeester, 2003). Since the operating temperatures of these membranes correspond to those required for the POM-reaction, integration of air separation and POM-reaction into a single apparatus seems very attractive. Furthermore, due to the O_2 consumption by the POM reaction the O_2 concentration is strongly reduced, which results in a high driving force over the membrane and a high accompanying permeation flux. Also, because the permeation rate through perovskites is related to the difference in chemical potential of oxygen over the membrane, the air side can be operated at atmospheric pressures, while higher pressures can be used at the syngas side. The integration of a perovskite membrane and the POM reaction in an isothermal reactor has already been studied by a number of authors (e.g. Balachandran et al., 1995).

The integration of air separation and the POM reaction has a major impact on the heat management of such a catalytic membrane reactor, since air, containing large amounts of inert N_2, will have to be pre-heated to the high reaction temperatures. To show the implication of the integration of air separation and the POM reaction an adiabatic thermodynamic analysis was carried out (Smit et al., 2004). The results of this adiabatic thermodynamic analysis are briefly discussed in the next section. Because a Fischer-Tropsch reactor is operated at much lower temperatures (± 500 K) than used in the POM-reactor, regenerative heat exchange is essential for air-based POM processes. Since external heat transfer at elevated temperatures is very expensive, regenerative heat exchange is preferably also carried out inside the reactor.

Internal regenerative heat exchange can be achieved with the reverse flow concept. In a reverse flow reactor the flow direction of the gas phase through a fixed bed catalyst is periodically reversed, while the reactants are fed without any preheating. The periodic gas flow reversals result in relatively low inlet and outlet temperatures with high temperatures in the centre of the reactor. A reverse flow reactor for the production of syngas has already been studied by Blanks et al. (1990) and was also studied by other authors (De Groote et al., 1996; Gosiewski et al., 1999), however in those studies air separation was not integrated in the reactor. In this work a novel multi-functional reactor is proposed called the Reverse Flow Catalytic Membrane Reactor (RFCMR) where the POM reaction, the air separation and the regenerative heat exchange are combined into a single apparatus. The concept is schematically depicted in Figure 1. With this new concept higher overall energy efficiencies are aimed at through process intensification.

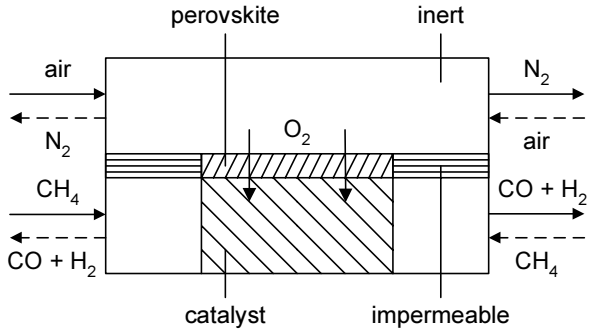

Figure 1. Schematic overview of the novel reactor concept.

The RFCMR consists basically of two compartments (e.g. shell-and-tube configuration) separated by a perovskite membrane in the centre of the reactor and impermeable walls at the in- and outlet. One compartment (e.g. shell side) is fed with CH_4 to be converted to syngas and the other compartment with air (e.g. tube side). The centre of the syngas compartment is filled with catalyst particles to carry out the POM reaction, while at the in- and outlets inert material is positioned to store energy and to prevent back-reactions. Also the air compartment is filled with inert material for additional heat capacity. The flow direction of the gas streams through both compartments is periodically reversed where the air and CH_4 feed are operated co-currently. Ideally the RFCMR has steep temperature gradients in the inert in- and outlet sections and a relatively flat temperature profile along the membrane to avoid membrane stability problems and to assure a constant O_2 flux through the membrane.

The aim of this paper is to investigate the feasibility of the reverse flow catalytic membrane reactor concept. Firstly the importance of regenerative heat exchange is demonstrated with an adiabatic thermodynamic analysis. Subsequently reactor models used to simulate the reactor behaviour are shortly presented. Based on the simulation results the reactor concept is elaborated and its feasibility demonstrated.

2 ADIABATIC THERMODYNAMIC ANALYSIS OF POM

In most thermodynamic studies published in the literature on POM processes the system was considered isothermally (e.g. Foulds and Lapszewicz, 1994; Zhu et al., 2001). Because the overall POM reaction is only slightly exothermic (-22.8 kJ/mol at 1000 K) the feed is usually preheated before feeding it to the POM reactor and some excess O_2 is used to generate additional heat (Aasberg-Petersen et al., 2001), indicating the importance of considering the reactor as an adiabatic reactor, rather than an isothermal reactor. When using air instead of pure O_2 as a feed, the required preheat duty is much higher, since the molar flow is more than doubled. Therefore, an adiabatic thermodynamic analysis has been carried out for an air-based POM process to investigate the implications of the integration of the air separation on the heat management, see also Smit et al. (2004). Adiabatic equilibrium calculations were carried out using Gibbs's free energy minimisation (Smith and Missen, 1982). Besides the reactants methane and oxygen and the products carbon monoxide and hydrogen from equation (1), also possible side products such as solid carbon (Boudouard reaction) and carbon dioxide and steam (full combustion of methane) have been considered. An overview of possible reactions that might occur in POM processes has been given by De Groote et al. (1996). Nevertheless, the equilibrium composition can be calculated from the initial composition, pressure and feed temperature without explicitly specifying the reactions occurring. It should be noted here that in the present study pure CH_4 is considered as a feedstock, whereas in practice natural gas will also contain minor amounts of other gaseous species. Nitrogen was accounted for only in the energy balance. Similar adiabatic studies have been performed by Chan and Wang (2000) and by Seo et al. (2002), but their studies were restricted to air/CH_4 mixtures at atmospheric pressures. To evaluate the air-based POM processes the relative molar syngas yield $CO + H_2$ (based on the initial amount of CH_4, optimally equal to 3), the relative molar carbon yield C (cokes formation, based on the initial amount of CH_4) and the molar H_2/CO ratio (syngas quality, optimally equal to 2) have been considered.

The importance of preheating of the feed in a stoichiometric air-based POM processes is illustrated in Figure 2, where the syngas and carbon yield and the H_2/CO ratio have been plotted as a function of the feed temperature (T_{feed}) for different operating pressures (p). With low feed temperatures and at low pressures the syngas yield and the H_2/CO ratio are reasonably, however, formation of cokes can be expected. To achieve a higher syngas yield without the possibility of coke formation high feed temperatures are required, especially at higher operating pressures. For a stoichiometric POM process at operating pressures typically encountered in GTL-processes, (> 20 bar; e.g. Aasberg-Petersen et al., 2001) very high feed temperatures are thus required in order to obtain a high syngas yield. The slow increase of the syngas yield with increasing feed temperature can be explained by the fact that at low feed temperatures relatively large amounts of CO_2 and H_2O are formed and accordingly a large amount of reaction heat is released (combustion) resulting in a large adiabatic temperature rise (see Figure 3). At higher feed temperatures mainly H_2 and CO are formed with a correspondingly lower adiabatic temperature rise.

To decrease the required feed temperature excess air could be fed to supply some additional heat. In Figures 4 and 5 the syngas and carbon yield and the H_2/CO ratio are plotted as a function of the O_2/CH_4 ratio for different pressures and feed temperatures. It can be observed that the syngas yield shows an optimum for an O_2/CH_4

ratio of about 0.7-0.8 giving a H_2/CO ratio of about 1.8 depending on the feed temperature and operating pressure. For higher feed temperatures and/or lower pressures higher syngas yields and somewhat higher H_2/CO ratios can be obtained with lower O_2/CH_4 ratios. The syngas yield and H_2/CO ratio can thus be optimised by selecting the appropriate feed temperature, operating pressure and O_2/CH_4 ratio. However, the improvement in the syngas yield by using excess air is modest and still very high feed temperatures are required to obtain acceptable syngas yields.

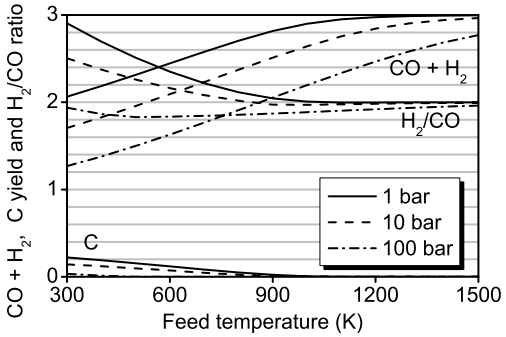

Figure 2. Syngas and carbon yield and H_2/CO ratio vs. feed temperature for different pressures. ($O_2/CH_4 = 0.5$)

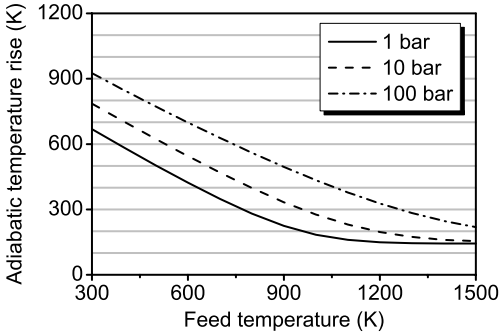

Figure 3. Adiabatic temperature rise vs. feed temperature for different pressures. ($O_2/CH_4 = 0.5$)

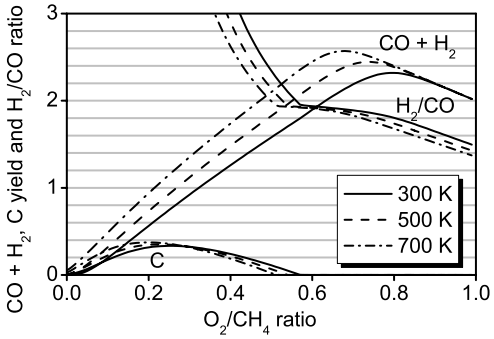

Figure 4. Syngas and carbon yield and H_2/CO ratio vs. O_2/CH_4 ratio for different feed temperatures. ($p = 20$ bar)

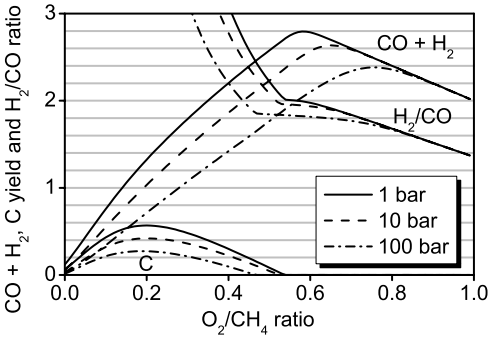

Figure 5. Syngas and carbon yield and H_2/CO ratio vs. O_2/CH_4 ratio for different pressures. ($T_{feed} = 700$ K)

It has been shown that very high feed temperatures are required for air-based POM processes to reach high syngas yields, especially at higher operating pressures. Because the Fischer-Tropsch reactor is typically operated at much lower temperatures (± 500 K) than the POM-reactor, recuperative heat exchange is indeed essential for air-based POM processes. Since external heat transfer at elevated temperatures is very expensive, the recuperative heat exchange is preferably also carried out inside the reactor. This can be achieved with the reverse flow concept as discussed in the introduction.

3 REACTOR MODEL

To study the feasibility of the RFCMR a reactor model is required to study its inherent dynamic behaviour. For this purpose a shell-and-tube reactor was selected as a possible configuration. In this section the reactor configuration and the model assumptions and equations are shortly discussed.

3.1 Reactor configuration

To study the RFCMR in further detail a shell-and-tube configuration with a square pitch was considered, illustrated in Figure 6. A cross-section close-up of the geometry is given in Figure 7. For the reactor model one unit cell is

considered, which is assumed to represent the entire tube bank. The geometry of the unit cell is thus determined by its width, the length of the non-permeable walls, the length of the membrane and the inner and outer tube radius.

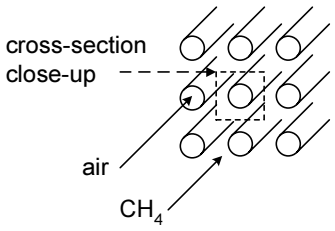

Figure 6. RFCMR geometry.

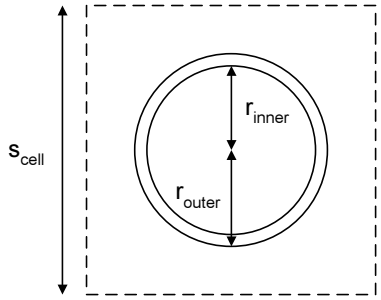

Figure 7. Cross-section close-up.

The aim of this paper is to provide a proof of principle with conceptual calculations and therefore some values for geometrical design parameters have been selected that are typically encountered in industrial practice. It is emphasised here that also other reactor configurations could be feasible or beneficial and the pitch, tube bank configuration, tube length, tube diameter etc. are design parameters that should be further optimised.

3.2 Reactor modelling and assumptions

The axial temperature and concentration profiles in the air and syngas compartments have been modelled with a 1-dimensional unsteady reactor model using the following general assumptions:

- Radial temperature and concentration gradients in the compartments have been ignored. In this study only the development of the axial temperature profiles were investigated to assess the over-all reactor performance.
- The heat capacity of the tube has been neglected, so that the heat transfer from the tube to the shell side could be assumed to be infinitely fast. To reduce computer effort a homogeneous model is adopted for the conservation of energy equation, following Vortmeyer (1989) and Nieken et al. (1995).
- The gas phase has been assumed to be in pseudo stationary-state because of the small gas residence time compared to the switching times, i.e. the accumulation terms of mass could be neglected and switching losses could be ignored.
- Axial mass dispersion could be neglected because of the high L/d_p ratio (> 100) considered in this work (Westerterp et al., 1984).
- The pressure drop has been neglected.

To model a conventional reverse flow reactor commonly two approaches are used; a dynamic model (DM) and a High Switching Frequency Model (HSFM) (e.g. Nieken et al., 1995; van Sint Annaland et al., 2002). The DM consists of the unsteady-state continuity equations for total and species mass and energy (Bird et al., 2002) and provides detailed information about the dynamic behaviour of the reactor. In the HSFM it is assumed that the flow direction is switched infinitely fast so that a simplified model can be used. Because the HSFM reaches a static steady state whereas the DM reaches a periodic steady state, the HSFM results can be interpreted more easily and the model equations can be solved numerically much faster than the DM. As a result the HSFM is used for preliminary studies, since additional complexity due to movement of the heat fronts is avoided. With the DM the findings with the HSFM can be verified and the effects of the movement of the heat front can be studied in more detail. The general model equations of the DM and HSFM are listed in Table 1 and 2 (next pages), respectively. As the initial condition a uniform temperature profile was taken and the usual Danckwerts-type boundary conditions were assumed. On both sides all gaseous species that are likely to be present have been considered.

Table 1. Model equations for the Dynamic Model (DM).

Tube side

Continuity equations:

$$\frac{\partial\left(\rho_g^{tube} v_g^{tube}\right)}{\partial z} = -M_{O_2}\frac{2}{r_{inner}} J_{O_2} \tag{3}$$

$$\rho_g^{tube} v_g^{tube}\frac{\partial w_{j,g}^{tube}}{\partial z} = r_{j,g}^{tube} + w_{j,g}^{tube} M_{O_2}\frac{2}{r_{inner}} J_{O_2} \tag{4}$$

$$\rho_g^{tube} v_g^{tube}\frac{\partial w_{O_2,g}^{tube}}{\partial z} = r_{O_2,g}^{tube} - \left(1 - w_{O_2,g}^{tube}\right) M_{O_2}\frac{2}{r_{inner}} J_{O_2} \tag{5}$$

Energy equation:

$$\left(\varepsilon_g^{tube}\rho_g^{tube} C_{p,g}^{tube} + \left(1-\varepsilon_g^{tube}\right)\rho_s^{tube} C_{p,s}^{tube}\right)\frac{\partial T^{tube}}{\partial t} + \rho_g^{tube} v_g^{tube} C_{p,g}^{tube}\frac{\partial T^{tube}}{\partial z} = \frac{\partial}{\partial z}\left(\lambda_{eff}^{tube}\frac{\partial T^{tube}}{\partial z}\right) - \sum_j r_{j,g}^{tube} H_{j,g}^{tube} + \frac{2}{r_{inner}}\alpha_{tube-shell}\left(T^{shell} - T^{tube}\right) \tag{6}$$

Shell side

Continuity equations:

$$\frac{\partial\left(\rho_g^{shell} v_g^{shell}\right)}{\partial z} = M_{O_2}\frac{2\pi r_{inner}}{s_{cell}^2 - \pi r_{outer}^2} J_{O_2} \tag{7}$$

$$\rho_g^{shell} v_g^{shell}\frac{\partial w_{j,g}^{shell}}{\partial z} = r_{j,g}^{shell} - w_{j,g}^{shell} M_{O_2}\frac{2\pi r_{inner}}{s_{cell}^2 - \pi r_{outer}^2} J_{O_2} \tag{8}$$

$$\rho_g^{shell} v_g^{shell}\frac{\partial w_{O_2,g}^{shell}}{\partial z} = r_{O_2,g}^{shell} + \left(1 - w_{O_2,g}^{shell}\right) M_{O_2}\frac{2\pi r_{inner}}{s_{cell}^2 - \pi r_{outer}^2} J_{O_2} \tag{9}$$

Energy equation:

$$\left(\varepsilon_g^{shell}\rho_g^{shell} C_{p,g}^{shell} + \left(1-\varepsilon_g^{shell}\right)\rho_s^{shell} C_{p,s}^{shell}\right)\frac{\partial T^{shell}}{\partial t} + \rho_g^{shell} v_g^{shell} C_{p,g}^{shell}\frac{\partial T^{shell}}{\partial z} = \frac{\partial}{\partial z}\left(\lambda_{eff}^{shell}\frac{\partial T^{shell}}{\partial z}\right) - \sum_j r_{j,g}^{shell} H_{j,g}^{shell} + \frac{2\pi r_{inner}}{s_{cell}^2 - \pi r_{outer}^2}\alpha_{tube-shell}\left(T^{tube} - T^{shell}\right) \tag{10}$$

Table 2. Model equations for the High Switching Frequency Model (HSFM).

Tube side

Continuity equations, forward direction (→):

$$\frac{\partial\left(\rho_{g,\rightarrow}^{tube} v_{g,\rightarrow}^{tube}\right)}{\partial z} = -M_{O_2}\frac{2}{r_{inner}} J_{O_2,\rightarrow} \tag{11}$$

$$\rho_{g,\rightarrow}^{tube} v_{g,\rightarrow}^{tube}\frac{\partial w_{j,g,\rightarrow}^{tube}}{\partial z} = r_{j,g,\rightarrow}^{tube} + w_{j,g,\rightarrow}^{tube} M_{O_2}\frac{2}{r_{inner}} J_{O_2,\rightarrow} \tag{12}$$

$$\rho_{g,\rightarrow}^{tube} v_{g,\rightarrow}^{tube}\frac{\partial w_{O_2,g,\rightarrow}^{tube}}{\partial z} = r_{O_2,g,\rightarrow}^{tube} - \left(1 - w_{O_2,g,\rightarrow}^{tube}\right) M_{O_2}\frac{2}{r_{inner}} J_{O_2,\rightarrow} \tag{13}$$

For the backward direction the same equations apply but now with subscript ←.

Energy equation:

$$\begin{aligned}&\left(\frac{1}{2}\varepsilon_g^{tube}\left(\rho_{g,\rightarrow}^{tube} C_{p,g,\rightarrow}^{tube} + \rho_{g,\leftarrow}^{tube} C_{p,g,\leftarrow}^{tube}\right) + \left(1-\varepsilon_g^{tube}\right)\rho_s^{tube} C_{p,s}^{tube}\right)\frac{\partial T^{tube}}{\partial t} = \\ &-\frac{1}{2}\left(\rho_{g,\rightarrow}^{tube} v_{g,\rightarrow}^{tube} C_{p,g,\rightarrow}^{tube} + \rho_{g,\leftarrow}^{tube} v_{g,\leftarrow}^{tube} C_{p,g,\leftarrow}^{tube}\right)\frac{\partial T^{tube}}{\partial z} + \frac{\partial}{\partial z}\left(\lambda_{eff}^{tube}\frac{\partial T^{tube}}{\partial z}\right) \\ &-\frac{1}{2}\left(\sum_j r_{j,g,\rightarrow}^{tube} H_{j,g,\rightarrow}^{tube} + \sum_j r_{j,g,\leftarrow}^{tube} H_{j,g,\leftarrow}^{tube}\right) + \frac{2}{r_{inner}}\alpha_{tube-shell}\left(T^{shell} - T^{tube}\right)\end{aligned} \tag{14}$$

Shell side

Continuity equations, forward direction (→):

$$\frac{\partial\left(\rho_{g,\rightarrow}^{shell} v_{g,\rightarrow}^{shell}\right)}{\partial z} = M_{O_2}\frac{2\pi r_{inner}}{s_{cell}^2 - \pi r_{outer}^2} J_{O_2,\rightarrow} \tag{15}$$

$$\rho_{g,\rightarrow}^{shell} v_{g,\rightarrow}^{shell}\frac{\partial w_{j,g,\rightarrow}^{shell}}{\partial z} = r_{j,g,\rightarrow}^{shell} - w_{j,g,\rightarrow}^{shell} M_{O_2}\frac{2\pi r_{inner}}{s_{cell}^2 - \pi r_{outer}^2} J_{O_2,\rightarrow} \tag{16}$$

$$\rho_{g,\rightarrow}^{shell} v_{g,\rightarrow}^{shell}\frac{\partial w_{O_2,g,\rightarrow}^{shell}}{\partial z} = r_{O_2,g,\rightarrow}^{shell} + \left(1 - w_{O_2,g,\rightarrow}^{shell}\right) M_{O_2}\frac{2\pi r_{inner}}{s_{cell}^2 - \pi r_{outer}^2} J_{O_2,\rightarrow} \tag{17}$$

For the backward direction the same equations apply but now with subscript ←.

Energy equation:

$$\begin{aligned}&\left(\frac{1}{2}\varepsilon_g^{shell}\left(\rho_{g,\rightarrow}^{shell} C_{p,g,\rightarrow}^{shell} + \rho_{g,\leftarrow}^{shell} C_{p,g,\leftarrow}^{shell}\right) + \left(1-\varepsilon_g^{shell}\right)\rho_s^{shell} C_{p,s}^{shell}\right)\frac{\partial T^{shell}}{\partial t} = \\ &-\frac{1}{2}\left(\rho_{g,\rightarrow}^{shell} v_{g,\rightarrow}^{shell} C_{p,g,\rightarrow}^{shell} + \rho_{g,\leftarrow}^{shell} v_{g,\leftarrow}^{shell} C_{p,g,\leftarrow}^{shell}\right)\frac{\partial T^{shell}}{\partial z} + \frac{\partial}{\partial z}\left(\lambda_{eff}^{shell}\frac{\partial T^{shell}}{\partial z}\right) \\ &-\frac{1}{2}\left(\sum_j r_{j,g,\rightarrow}^{shell} H_{j,g,\rightarrow}^{shell} + \sum_j r_{j,g,\leftarrow}^{shell} H_{j,g,\leftarrow}^{shell}\right) + \frac{2\pi r_{inner}}{s_{cell}^2 - \pi r_{outer}^2}\alpha_{tube-shell}\left(T^{tube} - T^{shell}\right)\end{aligned} \tag{18}$$

3.3 Numerical solution technique

Simulations of reverse flow reactors are computationally very demanding because of the very long (real-) time ($> 1 \cdot 10^5$ s) required to reach the (periodic) steady-state. Therefore, an efficient numerical solution procedure has been developed, which uses higher order schemes for discretisation of the accumulation and convection terms and also uses automatic time step adaptation and local grid refinement. The partial differential equations that describe the reactor are discretised using the method of lines with a finite volume approach (Schiesser, 1991). For the time discretisation the 3rd order accurate, L-stable, Singly Diagonal Implicit Runge-Kutta (SDIRK) method is used (Alexander, 1977). Implicit time discretisation is employed to avoid the requirement of very small time steps because of numerical stability. The convection term is discretised with the Weighted Essentially Non Oscillatory (WENO) scheme (Liu et al., 1994), which has been derived for an unstructured grid. The implemented scheme is 3rd order accurate in regions with steep gradients and 5th order in regions with smooth gradients. To solve the (stiff) non-linear source terms implicitly the Newton-Rhapson method is used. Time step adaptation is carried out by comparing calculation results with a time step of Δt and calculation results with two sequential time steps of $\Delta t/2$. If the maximum error exceeds a certain threshold the time step is decreased and if the deviation is sufficiently small, the time-step is increased. The grid size is adapted according to the local smoothness of the solution by comparing the smoothness indicators obtained in the WENO procedure. If the solution is very smooth a grid point is removed and if the solution is not smooth a grid point is added.

4 DEVELOPMENT OF THE NOVEL REACTOR CONCEPT

In this section firstly the input parameters that have been used in the calculations are given as well as some additional remarks on the constitutive equations. Then the HSFM is used to simulate the RFCMR concept. Based on these calculation results some conceptual improvements are proposed. Finally, the HSFM and DM results of the improved concept are discussed to show the reactors' feasibility

4.1 Operating conditions and constitutive equations

The operating conditions, reactor geometry and physical properties selected for the simulations are listed in Table 3. Optimisation of these parameters is not considered here, but will be part of future work.

Table 3. Simulation input parameters.

d_p^*	0.005	m
ε_g^*	0.4	-
$L_{membrane}$	1	m
$L_{reactor}$	3	m
r_{outer}	0.025	m
r_{inner}	0.023	m
s_{cell}	0.0625	m
$C_{p,s}^*$	1000	J/kg/K
J_{O2}	0.0734	Mol/m^2/s
λ_{bed}^*	0.3	W/m/K
p^{shell}	20	bar
p^{tube}	1	bar
ρ_s^*	2000	kg/m^3
T_{feed}^*	300	K

*Used for the tube side and the shell side.

To close the model equations additional constitutive equations are required for the O_2 flux through the membrane and the partial oxidation kinetics. It has been found in literature (Dong et al., 2001; Shao et al., 2001) that the membrane transport rate and the reaction kinetics significantly influence each other. However no flux and kinetic rate expressions are currently available to describe these rates simultaneously. Since the O_2 concentration is likely to

be extremely low, it will be required to determine the O_2 flux and the partial oxidation kinetics at these very low O_2 concentrations simultaneously, which will be subject of further research. For this conceptual study it is assumed that the O_2 flux is constant over the entire membrane length and that it is independent of the local partial pressures of O_2 and the temperature. An O_2 permeation rate that has been identified as economically feasible and that has been demonstrated in the literature in a perovskite membrane reactor is about 10 $cm^3/cm^2/min$ (STP), corresponding with 0.0734 $mol/m^2/s$ (Dong et al., 2001; Shao et al., 2001). With these assumptions the inlet mass fluxes on the tube and the shell side for a stoichiometric over-all feed composition can be calculated from the total O_2 permeation rate as:

$$\rho_{g,in}^{tube} v_{g,in}^{tube} = \frac{2L_{membrane}}{r_{inner}} \frac{M_{O_2}}{w_{O_2,air}} J_{O_2} \tag{19}$$

$$\rho_{g,in}^{shell} v_{g,in}^{shell} = \frac{2\pi r_{inner} L_{membrane}}{s_{cell}^2 - \pi r_{outer}^2} 2M_{CH_4} J_{O_2} \tag{20}$$

The tube side inlet mass flux is increased by 10 % to avoid oxygen depletion. In this case the air inlet mass flux is 0.97 $kg/m^2/s$, the CH_4 inlet mass flux is 0.17 $kg/m^2/s$, which gives a maximum syngas mass flux of 0.35 $kg/m^2/s$.

The catalytic partial oxidation of CH_4 is known to be very fast at the considered reaction conditions (Hickman and Schmidt, 1992), but reliable kinetic rate expressions are not available. Because of the high temperatures along the membrane it is therefore assumed that the shell side reactions along the membrane are infinitely fast and immediately reaching equilibrium and that solid carbon is not formed. In order to determine the equilibrium compositions the following reactions have been considered:

Full combustion of methane (I):

$$CH_4 + 2O_2 \rightarrow CO_2 + 2H_2O \tag{21}$$

Steam reforming of methane (II):

$$CH_4 + H_2O \rightarrow CO + 3H_2 \tag{22}$$

CO_2 reforming of methane (III):

$$CH_4 + CO_2 \rightarrow 2CO + 2H_2 \tag{23}$$

The combustion of methane is assumed to be infinitely fast so that the reaction is mass transfer limited and therefore equal to half of the oxygen flux through the membrane:

$$R^I = \frac{\pi r_{inner}}{s_{cell}^2 - \pi r_{outer}^2} J_{O_2} \tag{24}$$

The steam and CO_2 reforming of methane are assumed to reach equilibrium instantly:

$$R^{II} = k_\infty^{II} p_{CH_4,g}^{shell} p_{H_2O,g}^{shell} \left(1 - \frac{\left(p_{H_2,g}^{shell}\right)^3 p_{CO,g}^{shell}}{\left(p_g^{\theta}\right)^2 p_{CH_4,g}^{shell} p_{H_2O,g}^{shell} K_{eq}^{II}} \right) \tag{25}$$

$$R^{III} = k_\infty^{III} p_{CH_4,g}^{shell} p_{CO_2,g}^{shell} \left(1 - \frac{\left(p_{H_2,g}^{shell}\right)^2 \left(p_{CO,g}^{shell}\right)^2}{\left(p_g^{\theta}\right)^2 p_{CH_4,g}^{shell} p_{CO_2,g}^{shell} K_{eq}^{III}} \right) \tag{26}$$

where the reaction rate constant k_∞ has been chosen sufficiently high to assure that locally equilibrium is reached. Although other reactions than equations (21)-(23) might occur such as equation (1), three independent reaction equations are sufficient to describe the equilibrium since there are six species and three elements. The reaction rates r_j of the different species can now be calculated from equations (24)-(26).

The effective thermal conduction λ_{eff} is calculated according to a homogeneous axial heat dispersion model (Vortmeyer, 1989) based on the heterogeneous model of Gunn and Misbah (1993):

$$\lambda_{eff} = \lambda_{bed} + \frac{Re\,Pr\,\lambda_g}{Pe_{ax}} + \frac{Re^2\,Pr^2\,\lambda_g}{6\left(1-\varepsilon_g\right)Nu} \tag{27}$$

The bed conductivity λ_{bed} was estimated at 0.3 W/m/K (Koning, 2002), although its value is small compared to convective contribution (ca. 7 W/m/K). Pe_{ax} and Nu are calculated according to Gunn and Misbah (1993). Physical properties are calculated according to Daubert and Danner (1985) and Reid et al. (1987).

4.2 HSFM results of the basic concept

The axial temperature profiles and concentrations in the steady state in the basic concept of the RFMR calculated with the HSFM with the operating conditions listed in Table 3 are presented in Figure 8 and 9 for different values of the effective thermal conductivity. In this figure and subsequent figures the membrane section is located between the dotted lines.

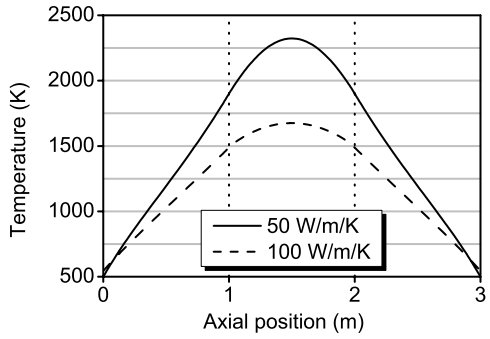

Figure 8. Axial temperature profile for the basic reactor concept for different values of the effective thermal conductivity (W/m/K), calculated with the HSFM.

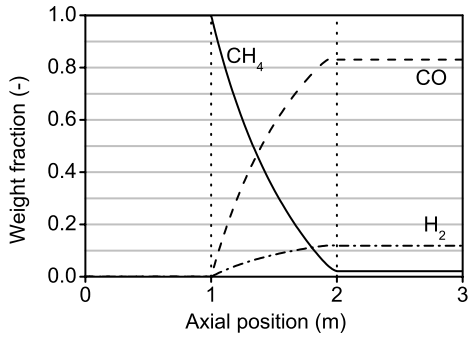

Figure 9. Axial profiles of the shell side weight fractions for the basic reactor concept, forward flow direction, calculated with the HSFM.
(λ_{eff} = 100 W/m/K)

For a reasonable effective thermal conductivity calculated with equation (27) (ca. 7 W/m/K, not shown in Figure 8) extremely high temperatures are calculated at the centre of the reactor. Due to the distributive addition of O_2 along the membrane length the reaction heat of the partial oxidation of CH_4 is released gradually. Because of the periodic flow reversal most of the energy is trapped at the centre of the membrane. Even with unrealistically high effective thermal conductivities the desired axial temperature profile with a uniform temperature profile over the membrane and the temperature gradients situated in the inert sections at the in- and outlet cannot be realised as is illustrated in Figure 8, although high syngas yields are obtained (Figure 9). The HSFM calculation results show that for the basic concept the O_2 membrane is exposed to extremely and unacceptable large temperature gradients and no temperature plateau in the centre of the reactor can be established. Moreover, in the actual dynamic situation, the movement of the temperature fronts will even deteriorate the situation. Furthermore in these calculations the O_2 permeation flux was assumed to be constant over the length of the membrane. Considering the fact that the O_2 permeation is an activated process the temperature gradients in the centre would actually even be steeper if the temperature dependence would have been accounted for, because at higher temperatures more oxygen permeates through the membrane and more reaction heat is released, while the opposite holds for lower temperatures. When comparing these results with conventional reverse flow reactors (e.g. Nieken et al., 1995), where no heat is released

in the centre of the reactor but only close to the inlets, steep temperature gradients at the in- and outlets can only be achieved in the RFCMR when reaction heat is actually produced in the inlet sections.

4.3 Conceptual improvements

To create the desired axial temperature profile in the RFCMR no net reaction heat should be released along the membranes and some reaction heat should be released at the inert sections at the in- and outlet.

Firstly to achieve isothermal conditions the produced reaction heat by the partial oxidation reactions should be removed along the membrane. This could for instance be achieved with the simultaneous production of steam by means of heat transfer tubes. However, very large heat transfer areas will be required, which would complicate the reactor design. Another possibility to maintain the centre of the RFCMR at isothermal conditions is the use of steam distributed along the O_2 membrane section. When feeding steam (≈ 10 % relative to the molar CH_4 feed) and increasing the CH_4 feed accordingly, some additional steam reforming (ΔH_r = 225 kJ/mol at 1000 K) takes place so that there is no over-all heat production in the centre of the reactor. Furthermore, some additional syngas is produced using the reaction heat of the partial oxidation reaction effectively. This steam injection can be achieved by using porous membranes/tubes positioned parallel the O_2 membranes or alternatively a number of "injection" tubes perpendicular to the perovskite membranes.

Secondly to create reverse flow behaviour it is required that a small amount of heat is released at the reactor inlet at the end of the temperature gradient in the inert section. It is proposed to combust a small amount of CH_4 according to equation (21) on the inlet of the air side.

Based on these considerations the original concept of the RFCMR is now modified to include distributive steam injection and CH_4 combustion at the air side. The modified concept is schematically depicted in Figure 10.

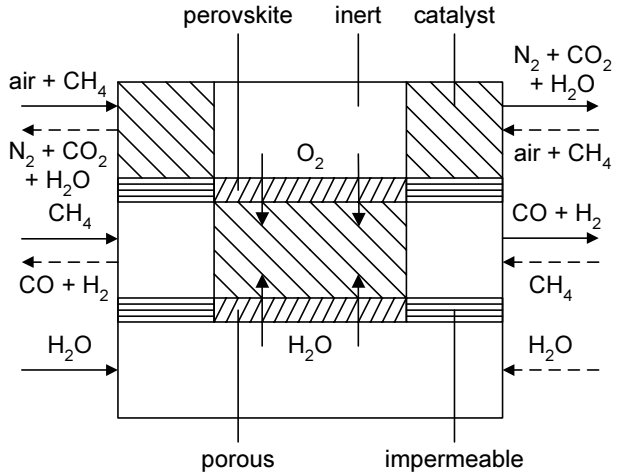

Figure 10. Schematic overview of the improved concept.

Distributive steam addition was taken into account via the source terms in the mass balances on the shell side. This is allowed since volumetric flow rates of steam are small compared to the CH_4 and air flows. Furthermore its influence on the reactor behaviour depends of the way the steam is injected. To account for the addition of steam the inlet mass flux of the shell side is adapted according to:

$$\rho_{g,in}^{shell} v_{g,in}^{shell} = \frac{2\pi r_{inner} L_{membrane}}{s_{cell}^2 - \pi r_{outer}^2} \frac{2M_{CH_4} J_{O_2}}{1 - R_{H_2O/CH_4}} \tag{28}$$

Here $R_{H2O/CH4}$ is defined as the ratio of the molar flow of H_2O that permeates through the porous membrane and the molar flow of CH_4 on the shell side. The total continuity of mass equation for the shell side is now given by:

$$\frac{\partial\left(\rho_g^{shell} v_g^{shell}\right)}{\partial z} = \frac{2\pi r_{outer}}{s_{cell}^2 - \pi r_{outer}^2}\left(\frac{r_{inner}}{r_{outer}} M_{O_2} J_{O_2} + M_{H_2O} J_{H_2O}\right) \tag{29}$$

The species continuity equations on the shell side are adjusted in a similar way. J_{H2O} is the (imaginary) permeation rate of steam based on the same surface area as the O_2 membranes, but defined on the shell side surface of the membrane. J_{H2O} is related to the shell side inlet mass flux via:

$$J_{H_2O} = R_{H_2O/CH_4} \frac{\rho_{g,in}^{shell} v_{g,in}^{shell}}{M_{CH_4}} \frac{s_{cell}^2 - \pi r_{outer}^2}{2\pi r_{outer} L_{membrane}} \tag{30}$$

To carry out methane combustion on the tube side the in- and outlets are filled with a Pt/γ-Al_2O_3 catalyst. The inlet mass flux on the tube side now has to be increased because of the addition of CH_4 according to:

$$\rho_{g,in}^{tube} v_{g,in}^{tube} = \frac{2L_{membrane}}{r_{inner}} \frac{J_{O_2}}{\frac{w_{O_2,air}}{M_{O_2}} - 2\frac{w_{CH_4,g,in}^{tube}}{M_{CH_4}}} \tag{31}$$

Again the species continuity equations on the tube side are adjusted analogously. The kinetics of the combustion of a small amount of methane in air has been determined in our laboratory for a 1.1 wt.% Pt/γ-Al_2O_3 monolith (van Sint Annaland, 2000). The reaction rate is given by:

$$r_{CH_4}^{tube} = -M_{CH_4} \eta^{tube} a_s^{tube} k_1^{tube} c_{CH_4,g}^{tube} c_{O_2,g}^{tube} e^{-\frac{E_a^{tube}}{R_g T^{tube}}} \tag{32}$$

The kinetic parameters are listed in Table 4 and correspond well with those obtained by Trimm and Lam (1980) for low concentrations of CH_4 in air (note that the reaction rate is given in terms of concentrations here). Other catalyst properties that have been used for the conceptual calculations have been included in Table 4.

Table 4. Catalyst properties.

k_1^{tube}	0.1608	$m^4/mol/s$
E_a^{tube}	$98.5 \cdot 10^3$	J/mol
a_s^{tube}	$1.0 \cdot 10^6$	m^2/m^3
ε_s^{tube}	0.6	-
τ^{tube}	2	-

Because the CH_4 fraction is small on the air side and because the O_2 fraction is almost constant at the combustion reaction zone at the inlet sections of the reactor, the reaction can be considered as a pseudo first order reaction with respect to methane. In case external mass transfer limitations can be neglected the effectiveness factor η^{tube} is given by (Westerterp et al., 1984):

$$\eta^{tube} = \frac{3\varphi^{tube} - tanh\left(3\varphi^{tube}\right)}{3\left(\varphi^{tube}\right)^2 tanh\left(3\varphi^{tube}\right)} \tag{33}$$

Where φ^{tube} is the Thiele modulus, defined as:

$$\varphi^{tube} = \frac{d_p^{tube}}{6}\sqrt{\frac{k_2^{tube}}{D_{s,eff}^{tube}}} \tag{34}$$

and k_2^{tube} (s^{-1}) is the apparent first order reaction rate constant, defined as:

$$k_2^{tube} = a_s^{tube} k_1^{tube} c_{O_2,g}^{tube} e^{-\frac{E_a^{tube}}{R_g T^{tube}}} \tag{35}$$

The effective diffusivity in inside the catalyst particle $D_{s,eff}^{tube}$ can be estimated with:

$$D_{s,eff}^{tube} = \frac{\varepsilon_s^{tube}}{\tau^{tube}} D_{CH_4}^{tube} \tag{36}$$

approximating the diffusivity of CH_4 in air $D_{CH4,air}^{tube}$ with the Fuller equation (Reid et al., 1987).

4.4 HSFM results of the improved concept

Using the modifications listed above, calculations with the HSFM for the improved concept revealed that the temperature plateau could indeed be controlled with the tube side CH_4 inlet weight fraction (0.0025) and that a flat temperature profile could be created keeping the centre of the reactor at more or less isothermal conditions. In Figure 11 the axial temperature profile is plotted for two different values of the relative steam injection flow rate $R_{H2O/CH4}$ and the accompanying shell side weight fraction profiles of CH_4, CO and H_2 for the forward direction are given in Figure 12.

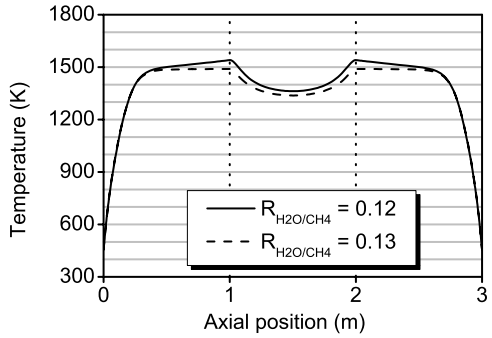

Figure 11. Axial temperature profile for the improved reactor concept for different values of $R_{H2O/CH4}$, calculated with the HSFM. ($w_{CH4,tube,in}$ = 0.0025)

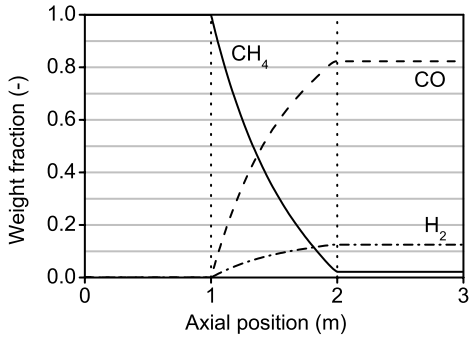

Figure 12. Axial profiles of the shell side weight fractions for the improved reactor concept, forward flow direction, calculated with the HSFM. ($R_{H2O/CH4}$ = 0.13; $w_{CH4,in}^{tube}$ = 0.0025)

It was found that with the improved reactor concept a high syngas yield (as defined in section 2) of 2.92 can be obtained based on the total feed of CH_4 ($R_{H2O/CH4}$ = 0.13) with a H_2/CO ratio of 2.11. Due to the addition of a small amount of steam the maximum syngas yield and the maximum H_2/CO ratio have increased slightly from 2 and 3 for pure POM to 3.13 and 2.13 ($R_{H2O/CH4}$ = 0.13), but this does not influence the results significantly. To improve the syngas yield even further higher temperatures can be applied in the centre, so that the conversion of methane on the shell side will be higher. Furthermore a lower activity of the combustion catalyst can be used or inert sections at the beginning of the air side to decrease the amount of methane that has to be fed to the air side (e.g. van Sint Annaland, 2000).

The axial temperature profile is not completely flat in the membrane section, which is caused by the changing equilibrium compositions along the membrane and incomplete conversion of CH_4. At higher temperatures only syngas is formed, as was shown in the adiabatic thermodynamic analysis, which will flatten the temperature profile, but higher temperatures are probably not feasible due to membrane stability constraints. Another possibility

to create better isothermal conditions at the membrane section is via a better tuning of the local steam and O_2 fluxes across the membranes. Alternatively the porous membranes for steam supply could be positioned perpendicularly to the perovskite membranes.

For conventional reverse flow reactors approximate relations for the plateau temperature and the gradient of the temperature front can be derived from the HSFM (e.g. Nieken et al., 1995; van Sint Annaland et al., 2002). For a hypothetical reactor consisting of two separated compartments with co-current flow and with a reaction occurring in one of the compartments similar expressions can be derived, if radial gradients can be ignored. In case of a geometry similar to that of the RFCMR the plateau temperature can be estimated by the following implicit equation:

$$\int_{T_{feed}+\Delta T_{ad}}^{T_{plateau}} k_3^{tube}\,dT = -\frac{\pi r_{inner}^2}{s_{cell}^2-\pi r_{outer}^2+\pi r_{inner}^2}\frac{\left(\rho_{g,in}^{tube}v_{g,in}^{tube}\right)^2\Delta H_r^{tube}w_{CH_4,g,in}^{tube}}{2\left\langle\lambda_{eff}\right\rangle M_{CH_4}} \tag{37}$$

Here ΔT_{ad} is given by:

$$\Delta T_{ad} = -\frac{\pi r_{inner}^2}{s_{cell}^2-\pi r_{outer}^2+\pi r_{inner}^2}\frac{\rho_{g,in}^{tube}v_{g,in}^{tube}\Delta H_r^{tube}w_{CH_4,g,in}^{tube}}{\left\langle\rho_{g,in}v_{g,in}C_{p,g}\right\rangle M_{CH_4}} \tag{38}$$

where the reaction rate constant k_3^{tube} is defined as:

$$k_3^{tube} = \frac{M_{CH_4}\eta^{tube}a_s^{tube}k_1^{tube}c_{CH_4,g}^{tube}c_{O_2,g}^{tube}e^{-\frac{E_a^{tube}}{R_gT^{tube}}}}{w_{CH_4,g}} \tag{39}$$

The average quantities in brackets are given by:

$$\left\langle Y\right\rangle = \frac{\left(s_{cell}^2-\pi r_{outer}^2\right)Y^{shell}+\pi r_{inner}^2Y^{tube}}{s_{cell}^2-\pi r_{outer}^2+\pi r_{inner}^2} \tag{40}$$

The adiabatic temperature rise was estimated (based on the inlet heat capacities) to be 82 K ($R_{H2O/CH4}$ = 0.13, $w_{CH4,tube,in}$ = 0.0025), which is lower than the value found in the simulation (156 K). This is because of the varying physical properties throughout the reactor and because some reaction heat is produced in the centre of the reactor. If this reaction heat is taken into account and if the adiabatic temperature rise is based on the outlet conditions a better estimation can be made (170 K). Moreover, it was found that the temperature at the end of the steep part of the temperature profile could be predicted reasonably well (1503 K predicted by Equation (37) vs. 1490 K from the numerical simulation) taking the inlet mass fluxes and by approximating the heat capacities and the effective thermal conductivity at 900 K. Nevertheless, Equation (37) can be used to get an indication of the required inlet fraction of CH_4 to achieve the desired plateau temperature.

4.5 DM results of the improved concept

To verify the possibility of the improved concept under dynamic conditions, simulations have been carried out with the DM using the same operating conditions and physical properties as for the HSFM simulations shown before. For the simulations the cycle time between switching of flow directions was set at 400 s. The resulting axial temperature profiles at the end of the forward (→) and backward (←) cycles in the periodic steady state are presented in Figure 13. The corresponding outlet weight fractions of CO and H_2 during a number of cycles are shown in Figure 14.

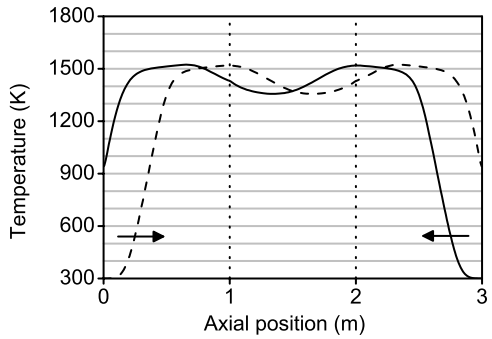

Figure 13. Axial temperature profile for the improved reactor concept, calculated with the DM. ($R_{H2O/CH4}$ = 0.13; $w_{CH4,in}^{tube}$ = 0.0025)

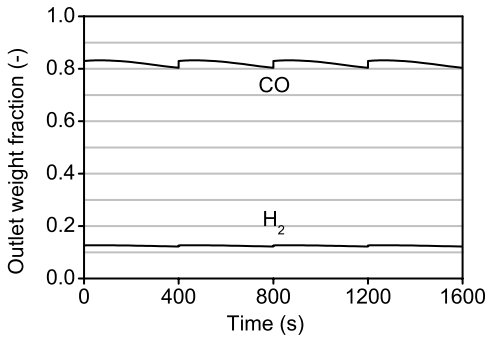

Figure 14. Shell side H_2 and CO outlet weight fractions vs. time for a number of cycles for the improved reactor concept, calculated with the DM. ($R_{H2O/CH4}$ = 0.13; $w_{CH4,in}^{tube}$ = 0.0025)

The simulations results clearly show that high temperatures are maintained in the membrane section during the entire cycles while the temperature gradients remain steep in the in- and outlet sections. However the temperatures at the outlets at the end of a cycle are high for the selected operating conditions, which would require expensive construction materials for the switching valves. A possible way to eliminate the high temperatures at the end of the cycles is by using less active sections at the in- and outlet sections of the air compartment and using a lower CH_4 inlet fraction (van Sint Annaland, 2000). The resulting lower adiabatic temperature rise decreases the slope of the temperature front simultaneously reducing the maximum temperature outlet temperature during the cycle. By tuning the catalyst activity the desired maximum temperature can be achieved. The outlet weight fractions of CO and H_2 on the shell side remain fairly constant during a cycle and the time-averaged syngas yield is 2.92, which is the same as was calculated with the HSFM. The H_2/CO ratio is 2.11, which is also the same as calculated with the HSFM. Apparently, the syngas yield is somewhat higher at the beginning of a cycle due to the higher temperatures at the end of the membrane section and somewhat lower at the end of the cycle because of lower temperatures at the outlet compared to the HSFM case. However the temperature profile along the membrane at the centre of the reactor can be improved by optimising the local steam injection fluxes.

The velocity of the temperature front in a conventional reverse flow reactor can be derived from the DM (e.g. Froment, 1990). The velocity of the temperature front in the RFCMR can be approximated in a similar way as was discussed before for the plateau temperature and is given by:

$$v_{front} = \frac{\left\langle \rho_{g,in} v_{g,in} C_{p,g} \right\rangle}{\left\langle \left(1-\varepsilon_g\right)\rho_s C_{p,s} + \varepsilon_g \rho_g C_{p,g} \right\rangle} \left(1 - \frac{\Delta T_{ad}}{T_{plateau} - T_{feed}} \right) \tag{41}$$

Approximating the heat capacities and densities at 900 K, the front velocity was estimated to be $7.2 \cdot 10^{-4}$ m/s, which corresponds quite well with the DM results ($9.3 \cdot 10^{-4}$).

5 CONCLUSIONS

An adiabatic thermodynamic analysis of an air-based POM process revealed that the integration of air separation and the POM into a novel reactor has a major impact on the heat management. For an air-based process very high feed temperatures are required in order to obtain high syngas yields. Adding excess air in the feed can reduce this required feed temperature to some extent, but still very high feed temperatures are required, so that regenerative heat exchange is essential for air-based processes. A novel reactor concept, referred to as the Reverse Flow Catalytic Membrane Reactor has been proposed, which combines the POM reaction, the air separation and the regenerative heat exchange into a single apparatus.

Calculations with the HSFM showed that for the basic RFCMR concept unacceptably high temperatures are obtained in the centre of the reactor due to the gradual heat production along the membrane. The desired

temperature profile with a uniform temperature along the membrane and the temperature fronts located at the in- and outlet sections could not be achieved, not even for unrealistically high effective thermal conductivities. To maintain the membrane section at isothermal conditions it is proposed to insert an additional porous membrane along or perpendicular to the perovskite membrane for distributive feeding of a small amount of steam. Additionally, a small amount of CH_4 should be combusted at the air side to create the desired temperature profile with the temperature fronts located in the in- and outlet sections. HSFM calculations showed that with these modifications the desired temperature profile could indeed be accomplished. Better isothermal conditions can be achieved via tuning of the local steam injection profile. DM calculations demonstrated that the RFCMR can also be operated with reasonable cycle times. The high outlet temperatures at the end of a cycle can be reduced via optimisation of the CH_4 inlet weight fraction and the catalyst activity at the air side. Analytical relations have been derived to estimate the plateau temperature and the front velocity in the RFCMR.

In the reactor model assumptions have been made, which need to be studied in further detail. Especially interaction between the perovskite membrane and the POM reaction and the way the O_2 flux and the reaction kinetics are influenced by each other need to be studied in further detail (experimentally) and will be subject of further research. Also radial effects, shell side back reactions, tube side homogeneous gas phase reactions and possible coke formation need to be investigated further. In the HSFM and DM calculations the maximum temperature exceeded 1500 K. Such high temperatures are required to reach high syngas yields at elevated pressures from a thermodynamic point of view, assuming an overall undiluted stoichiometric feed. Therefore the operating conditions were chosen to obtain these high temperatures and to demonstrate the reactor concept. However, so far no perovskite membranes have been reported that can operate above 1200 K (Bouwmeester, 2003) and major technical hurdles have yet to be overcome. The maximal allowed temperature and the maximal allowed pressure difference over the membrane will determine the operating conditions of the RFCMR in practice.

ACKNOWLEDGEMENTS

The authors gratefully acknowledge the financial support of the Dutch Technology Foundation STW, the Energy research Centre of the Netherlands ECN and the Association of Industrial Advisory Council Members of the Dutch Institute for Catalysis Research VIRAN.

NOTATION

a_s	internal surface area of catalyst particle, m^2/m^3
c_j	concentration of species j, mol/m^3
C_p	Heat capacity, J/kg/K
d_p	particle diameter, m
$D_{CH4,air}$	effective diffusivity of CH_4 in air, m^2/s
$D_{s,eff}$	effective diffusivity inside catalyst particle, m^2/s
E_a	activation energy, J/mol
ΔH_r	Reaction enthalpy, J/mol
H_j	enthalpy of species j, J/kg
J_{O2}	O_2 flux through membrane defined at tube side, $mol/m^2/s$
J_{H2O}	H_2O flux through membrane defined at shell side, $mol/m^2/s$
k_1	reaction rate constant, $m^4/mol/s$
k_2	reaction rate constant, s^{-1}
k_3	reaction rate constant, $kg/m^3/s$
k_∞	sufficiently high reaction rate constant, $mol/Pa^2/m^3/s$
K_{eq}	equilibrium constant
$L_{membrane}$	membrane length, m
$L_{reactor}$	reactor length, m
M_j	molar weight of species j, kg/mol
Nu	dimensionless Nusselt number

p	pressure, bar
p_j	partial pressure of species j, Pa
Pe_{ax}	dimensionless Péclet number for axial heat dispersion
Pr	dimensionless Prandtl number, $C_{p,g}\eta_g/\lambda_g$
r_{inner}	inner tube radius, m
r_{outer}	outer tube radius, m
r_j	reaction rate of species j, kg/m^3/s
$R_{H2O/CH4}$	ratio of added steam flow and shell side inlet CH_4 flow (molar based)
R	reaction rate, mol/m^3/s
R_g	gas constant, 8.314 J/mol/K
Re	dimensionless Reynolds number, $d_p\rho_g v_g/\eta_g$
s_{cell}	unit cell size, m
t	time, s
T	temperature, K
ΔT_{ad}	adiabatic temperature rise, K
T_{feed}	feed temperature, K
$T_{plateau}$	plateau temperature, K
v	superficial velocity based on compartment volume, m/s
v_{front}	front velocity, m/s
w_j	weight fraction of species j
$w_{O2,air}$	weight fraction of O2 in air (0.232)
Y	some quantity
z	axial coordinate, m

Greek Letters

$\alpha_{tube\text{-}shell}$	over-all heat transfer coefficient between tube and shell side, W/m^2/K
ε_g	gas phase porosity based on compartment volume
ε_s	catalyst particle porosity based on catalyst particle volume
η	effectiveness factor
η	viscosity, kg/m/s
φ	Thiele modulus
λ_{bed}	bed thermal conductivity, W/m/K
λ_{eff}	effective thermal conductivity, W/m/K
λ	thermal conductivity, W/m/K
ρ	density, kg/m^3
τ	tortuosity

Subscripts

g	gas phase
in	inlet
s	solid phase
$\rightarrow$	forward direction
$\leftarrow$	backward direction

Superscripts

I	methane combustion
II	steam reforming of methane
III	CO_2 reforming of methane
$\ominus$	at standard pressure
$shell$	shell side
$tube$	tube side

REFERENCES

Aasberg-Petersen, K., Bak Hansen, J.-H., Christensen, T.S., Dybkjaer, I., Seier, Christensen, P., Stub Nielsen, C., Winter Madsen, S.E.L., and Rostrup-Nielsen, J.R., "Technologies for Large Scale Gas Conversion", Appl. Catal. A-Gen., Vol. 221, No. 1-2, 379-387 (2001)

Alexander, R., "Diagonal Implicit Runge-Kutta Methods for Stiff O.D.E.'s", SIAM J. Numer. Anal., Vol. 14, No. 6, 1006-1021 (1977)

Balachandran, U., Dusek, J.T., Mieville, R.L., Poeppel, R.B., Kleefisch, M.S., Pei, S., Kobylinski, T.P., Udovich, C.A., and Bose, A.C., "Dense Ceramic Membranes for Partial Oxidation of Methane to Syngas", Appl. Cat. A-Gen., Vol. 133, No. 1, 19-29 (1995)

Bird, R.B., Stewart, W.E., and Lightfoot, E.N., "Transport Phenomena", 2nd Edition, John Wiley & Sons, New York (2002)

Blanks, R.F., Wittrig, T.S., and Peterson, D.A., "Bidirectional Adiabatic Synthesis Gas Generator", Chem. Eng. Sci., Vol. 45, No. 8, 2407-2413 (1990)

Bouwmeester, H. J. M., "Dense Ceramic Membranes for Methane Conversion", Catal. Today, Vol. 82, No. 1-4,141-150 (2003)

Chan, S.H., and Wang, H.M., "Thermodynamic Analysis of Natural-Gas Fuel Processing For Fuel Cell Applications", Int. J. Hydrogen Energ., Vol. 25, No. 5., 441-449 (2000)

Daubert, T.E., and Danner, R.P., "Data Compilation Tables of Properties of Pure Compounds", American Institute of Chemical Engineers, New York (1985)

Dong, H., Shao, Z., Xiong, G., Tong, J., Sheng, S., and Yang, W., "Investigation on POM Reaction in a New Perovskite Membrane Reactor, Catal. Today, Vol. 67, No. 103, 3-13 (2001)

Foulds, G.A., and Lapszewicz, J.A., "Catalytic Partial Oxidation of Methane to Synthesis Gas (Syngas)", Catalysis, Vol. 11, 412-440 (1994)

Froment, G.F., "Reverse Flow Operation of Fixed Bed Catalytic Reactors", in "Unsteady State Processes in Catalysis", Matros, Yu. Sh., Ed., VSP, Utrecht, 57-89 (1990)

Gosiewski, K., Bartmann, U., Moszcynski, M., and Mleczko, L., "Effect of the Intraparticle Mass Transport Limitations on Temperature Profiles and Catalytic Performance of the Reverse-Flow Reactor for the Partial Oxidation of Methane to Synthesis Gas", Chem. Eng. Sci., Vol. 54, No. 20, 4589-4602 (1999)

Groote, A.M. De, Froment., G.F. and Kobylinski, Th., "Synthesis Gas Production from Natural Gas in a Fixed Bed Reactor with Reversed Flow", Can. J. Chem. Eng., Vol. 74, No. 5, 735-742 (1996)

Gunn, D.J., and Misbah, M.M.A., "Bayesian Estimation of Heat Transport Parameters in Fixed Beds", Int. J. Heat Mass Transfer, Vol. 36, No. 8, 2209-2221 (1993)

Hickman, D.A., and Schmidt, L.D., "Synthesis Gas Formation by Direct Oxidation of Methane over Pt monoliths, J. Catal., Vol. 138, 267-282 (1992)

Koning, G.W., "Heat and Mass Transfer Transport In Tubular Packed Bed Reactors at Reacting Conditions And Non-Reacting Conditions: Experiments and Models", Ph.D. Thesis, University of Twente, Enschede, The Netherlands (2002)

Liu, X.D., Osher, S., and Chan, T., "Weighted Essentially Non-Oscillatory Schemes", J. Comp. Phys., Vol. 115, No. 1, 200-212 (1994)

Nieken, U., Kolios. G., and Eigenberger, G., "Limiting Cases and Approximate Solutions for Fixed-Bed Reactors with Periodic Flow Reversal", AIChE J., Vol. 41, No. 8, 1915-1925 (1995)

Prettre, M., Eichner, C., and Perrin, M., "The Catalytic Oxidation of Methane to Carbon Monoxide and Hydrogen", Trans. Faraday Soc., Vol. 43, 335-340 (1946)

Reid, R.C., Prausnitz, J.M., and Poling, B.E., "The Properties of Gases and Liquids", 4th Edition, McGraw-Hill, Inc., New York (1987)

Rostrup-Nielsen, J.R., "Syngas in Perspective", Catal. Today, Vol. 71, No. 3-4, 243-247 (2002)

Schiesser, W.E., "The Numerical Method of Lines: Integration of Partial Differential Equations", Academic Press, San Diego (1991)

Seo, Y. -S., Shirley, A. and Kolaczkowski, S. T., "Evaluation of Thermodynamically Favourable Operating Conditions for Production of Hydrogen in Three Different Reforming Technologies", J. Power Sources, Vol. 108, No. 1-2, 213-225 (2002)

Shao, Z., Xiong, G., Dong, H., Yang, W., and Lin, L., "Synthesis, Oxygen Permeation Study and Membrane Performance of a Ba(0.5)Sr(0.5)Co(0.8)Fe(0.2)O(3) Oxygen-Permeable Dense Ceramic Reactor for Partial Oxidation of Methane to Syngas, Sep. Purif. Technol., Vol. 25, No. 1-3, 97-116 (2001)

Sint Annaland, M. van, "A Novel Reverse Flow Reactor Coupling Endothermic and Exothermic Reactions", Ph.D. Thesis, University of Twente, Enschede, The Netherlands (2000)

Sint Annaland, M. van, Scholts, H. A. R., Kuipers, J. A. M., and Swaaij, W. P. M. van, "A Novel Reverse Flow Reactor Coupling Endothermic and Exothermic Reactions. Part I: Comparison of Reactor Configurations for Irreversible Endothermic reactions", Chem. Eng. Sci., Vol. No. 5, 833-854 (2002)

Smit, J., Sint Annaland, M. van, and Kuipers, J.A.M., "Development of a novel reactor concept for the partial oxidation of methane", Accepted for publication in Chem. Eng. Res. Des. (2004)

Smith, W.R., and Missen, R.W., "Chemical Reaction Equilibrium Analysis: Theory and Algorithms", John Wiley & Sons, New York (1982)

Trimm, D.L, and Lam, C.-W., "The Combustion of Methane on Platinum-Alumina Fibre Catalysts-1: Kinetics and Mechanism", Chem. Eng. Sci., Vol. 35, No. 6, 1405-1413 (1980)

Westerterp, K.R., van Swaaij, W.P.M., and Beenackers, A.A.C.M., "Chemical Reactor Design and Operation", John Wiley and Sons, New York (1984)

Vortmeyer, D., "Packed Bed Thermal Dispersion Models and Consistent Sets of Coefficients", Chem. Eng. Process., Vol. 26, 263-268 (1989)

Zhu, J., Zhang, D., and King, K.D., "Reforming of CH4 by Partial Oxidation: Thermodynamic and Kinetic Analyses", Fuel, Vol. 80, No. 7, 899-903 (2001)